08

Studies of $Al_xGa_{1-x}N$/AlN, nanosized columnar heterostructures grown on silicon substrates with various surface modifications

© P.V. Seredin,[1] A.M. Mizerov,[2] N.A. Kurilo,[1] S.A. Kukushkin,[2,3] D.L. Goloshchapov,[1] N.S. Buylov,[1] A.S. Len'shin,[1] D.N. Nesterov,[1] M.S. Sobolev,[2] S.N. Timoshnev,[2] K.Yu. Shubina[2]

[1] Voronezh State University,
394018 Voronezh, Russia
[2] Saint Petersburg National Research Academic University of the Russian Academy of Sciences,
194021 St. Petersburg, Russia
[3] Institute of Problems of Mechanical Engineering, Russian Academy of Sciences,
199178 St. Petersburg, Russia
e-mail: paul@phys.vsu.ru

Received May 23, 2023
Revised September 8, 2023
Accepted October 23, 2023

The growth of nanosized columnar $Al_xGa_{1-x}N$/AlN heterostructures on the surface of silicon substrates of three types, namely, on a standard atomically smooth *c*-Si substrate, a Si substrate with a transition layer of porous silicon por-Si/*c*-Si, and a hybrid a substrate containing a layer of silicon carbide grown by the method of coordinated substitution of atoms on the surface of porous silicon SiC/por-Si/*c*-Si. The complex structural-spectroscopic analysis carried out showed that the epitaxial growth of the AlN nucleation layer on all types of substrates under N-enriched conditions leads to the formation of $Al_xGa_{1-x}N$/AlN heterostructures with a Ga-polar surface. It was found that a layer of an ordered $Al_xGa_{1-x}N$ solid solution was formed only on the SiC/por-Si/*c*-Si hybrid substrate. On *c*-Si and por-Si/*c*-Si substrates, the $Al_xGa_{1-x}N$ layer is in the state of a disordered solid solution with an excess content of gallium atoms. It has been demonstrated that $Al_xGa_{1-x}N$ nanosized columns formed on a SiC/por-Si/*c*-Si substrate are tilted relative to the *c*-axis, which is associated with the peculiarities of the formation of the SiC layer by the method of coordinated substitution of atoms on a porous Si substrate, which leads to the formation of inclined (111) SiC facets. at the interface between the (111) Si surface and pores in Si. Optical studies of the grown samples showed that the optical band-to-band transition for the $Al_xGa_{1-x}N$ solid solution with $E_g = 3.99$ eV was observed only when studying the heterostructure grown on the SiC/por-Si/*c*-Si substrate. The results obtained in this work demonstrate the promise of using SiC/por-Si/*c*-Si substrates for the integration of silicon technology and the technology of synthesizing nanosized $Al_xGa_{1-x}N$ columnar heterostructures by molecular beam epitaxy with nitrogen plasma activation.

Keywords: nanosized columnar $Al_xGa_{1-x}N$/AlN heterostructures, epitaxial growth, porous silicon, silicon carbide, pliable substrate.

DOI: 10.61011/JTF.2024.01.56912.135-23

Introduction

The active development of approaches to epitaxial growth of heterostructures based on semiconductor compounds of nitrides of the third group ($A_{III}N$) allows designing and manufacturing devices covering a wide range of applications: UHF high electron mobility transistor (HEMT), LEDs in the UV, visible and IR spectral regions (LED), detectors for a voltage-modulated light source, etc. [1,2]. The integration of $A_{III}N$ semiconductor materials with a silicon signal processing circuit provides a broad field of opportunities for the development of new functional devices [3–5]. In particular, the creation of electromagnetic radiation sources based on nitride compounds formed on a silicon substrate can significantly expand the capabilities of silicon photonics and launch optical data transmission directly inside the microcircuits [6].

The absence of polarity in Si substrates allows growing both Ga- and N-polar structures based on GaN on Si. It is well known that two-dimensional Ga-polar heterostructures grown by gas-phase epitaxy from metal-organic compounds (GPE MOC) [7] are usually used in most instrument structures, since they usually have the best morphological and electrophysical characteristics. However, there are a number of applications where N-polar compounds have the advantages [8,9]. For this reason, more and more attention has recently been paid to the issues of polarity control in the epitaxial synthesis of compounds $A_{III}N$. We have already shown the possibility of growing GaN layers with both Ga- and N-polarity on silicon substrates by molecular-beam epitaxy with plasma activation of nitrogen (PA MBE) [10]. Additionally, we showed in [9],the potential possibility of separating the upper thick Ga-polar GaN layer grown by chloride hydride epitaxy from the SiC/Si(111) substrate by etching the intermediate GaN layer with the opposite N-polarity synthesized by PA MBE.

However, the problems of monolithic integration of photonic devices based on nitrides of the third group

with silicon substrates have not yet been solved. Recent studies show that some of these fundamental problems can potentially be solved by using $A_{III}N$ nanoscale structures (nanowhiskers, nanocrystals, nanocolumns), which are epitaxially grown on lattice mismatched substrates such as silicon and sapphire, and have a relatively high crystalline quality owing to the effective relaxation of elastic stresses because of three-dimensional island nucleation [11].

It is known that the PA MBE technology allows using various stoichiometric growth conditions characterized by the ratio of the intensities of the fluxes of atoms of the third group (F_{III}) and activated nitrogen (F_N) entering the growth surface and forming layers $A_{III}N$ both with a nanocolumn, and with smooth morphology without preepitaxial masking of the Si(111) [12] substrate. However, nitride compounds are also known to be grown in industrial PA MBE systems primarily using small streams of activated nitrogen, i.e. with low growth rates of $< 0.1\,\mu$m/h. This fact, on the one hand, suggests the possibility of precision control of layer thicknesses at the level of 1–2 monolayers during PA MBE synthesis of quantum-dimensional heterostructures based on GaN, on the other hand, low growth rates significantly limit the possibility of using thick buffer layers grown on substrates for reducing the density of defects in the upper layers of instrument epitaxial heterostructures. At the same time, for example, the prospects of using island ultrathin GaN nanostructures grown directly on silicon substrates by the PA MBE method for the creation of UV radiation detectors are demonstrated in [13]. We synthesized AlGaN/AlN island nanoheterostructures in our study which have a low aspect ratio unlike more popular nanostructures with a high aspect ratio, such as nanowhiskers, nanocolumns, etc. They were also grown without using thick epitaxial buffer layers for ensuring maximum efficiency and speed of the process of manufacturing of devices based on these materials, primarily UV radiation detectors. Thus, the purpose of this study was to study the possibility of epitaxial synthesis of ultrathin epitaxial AlGaN/AlN heterostructures with acceptable crystalline quality on silicon substrates with various surface modifications (smooth, porous, with an upper SiC layer) in a single growth process, i.e. in the closest possible growth conditions, and their comprehensive study.

We have recently completed a series of studies of the growth of nanocolumnar GaN layers synthesized on hybrid substrates SiC/por-Si/*c*-Si [14,15] by the PA MBE method that demonstrated the potential of this approach for integrating GaN technology with silicon electronics and the need for further studies in this area. For this reason the goal of this work is a comparative study of nanoscale columnar $Al_xGa_{1-x}N$-heterostructures grown by the PA MBE method on silicon substrates with various surface modifications: standard, atomically smooth *c*-Si, with a transition layer of porous silicon por-Si/*c*-Si, as well as a hybrid substrate containing a layer of silicon carbide grown on the surface of silicon SiC/por-Si/*c*-Si.

1. Materials and methods

$Al_xGa_{1-x}N$/AlN heterostructures were grown by molecular beam epitaxy with plasma activation of nitrogen (PA MBE) using industrial-type Veeco GEN200 MBE system in a single epitaxial process [16]. Standard growth experiments were performed before the growth of heterostructures for calibration of the main process parameters of the industrial system. Moving Bayard–Alpert ionization gauge with a measurement range from 10^{-3} to 10^{-9} Torr is used to monitor the stability and calibrate the equivalent pressures of aluminum (F_{Al}) and gallium (F_{Ga}) flows. This gauge during the measurement process is placed in front of the main shutter, i.e., almost at the location of the substrate. The temperatures of all types of substrates used in experiments were measured using IR pyrometer and a W–Re thermocouple (GaN/*c*-Al_2O_3, *c*-Si, por-Si/*c*-Si, SiC/por-Si/*c*-Si). It should be noted that the calibration procedure of the main process parameters of Veeco GEN200 PA MBE system used in the study is performed regularly to prevent their uncontrolled change and ensure stable reproducibility of the results, which was confirmed by calibration experiments for the growth of AlN and GaN layers on virtual substrates GaN/*c*-Al_2O_3. The PA MBE synthesis of GaN on virtual substrates of GaN/*c*-Al_2O_3 are described in [17].

In particular, virtual substrates GaN/*c*-Al_2O_3 in AlN and GaN growth rate units were used in calibration experiments for determination of fluxes of F_{Al}, F_{Ga} and F_N to minimize the mismatch of the crystal lattice parameters of the growing AlN and GaN layers with the substrate. Several process experiments were conducted for the growth of binary compounds AlN and GaN in metal-enriched environment ($F_{III} > F_N$) at the same substrate temperature ($T = 660^\circ$C), excluding active desorption of Ga and Al adatoms from the growth surface for determining the maximum flux of activated nitrogen. AlN or GaN layer was grown in each experiment with constant values of HF plasma source power and molecular nitrogen consumption. The values of HF power of the plasma source and the consumption of molecular nitrogen varied in the performed experiments. The thicknesses and, accordingly, the rates of growth of the obtained layers were determined using *ex-situ* canning electron microscopy measurements. It was found that the maximum value of the activated nitrogen flux achievable in the existing plant configuration is $F_N \sim 0.04–0.05\,\mu$m/h.

A similar approach was used to determine F_{Al} and F_{Ga} fluxes in units of AlN or GaN growth rate. AlN or GaN layers were grown in this case on virtual substrates GaN/*c*-Al_2O_3 using nitrogen-enriched environment ($F_{III} < F_N$) controlled *in-situ* based on the three-dimensional diffraction pattern of reflected fast electrons.

Si(111) substrates with various surface modifications were used for growing heterostructures $Al_xGa_{1-x}N$/AlN studied in the work: standard smooth *c*-Si substrates, Si(111) substrates with a porous layer formed on the por-*c*-Si surface, as well as SiC/por-Si/*c*-Si substrates, on the

surfaces of which SiC layer [18] was formed using the method of coordinated atomic substitution.

c-Si substrates were trained using the Shiraki method before the PA MBE synthesis of GaN. The por-Si and SiC/por-Si/*c*-Si substrates were degreased. Then all the substrates were loaded into one substrate holder of the PA MBE system, after which they were annealed in a pre-annealing chamber at 200°C.

Then the substrates were moved to the main growth chamber of the PA MBE system, where they first subjected to pre-epitaxial treatment comprising the nitridization of the substrate surfaces in a flux of activated nitrogen. It should be noted that the substrate nitridization was conducted in the described experiments with the nitrogen source choke closed, which, according to some literature data, can lead to the formation of a high-quality SiN layer on the surface of silicon substrates [19]. It should also be noted that the substrates containing the SiC layer do not react with nitrogen at this temperature, so they were annealed only for the „integrity" of the experiment.

The nitridization was performed at a substrate temperature measured by an IR pyrometer, $T \sim 670°C$ for 30 min. The parameters of plasma source (HF power and nitrogen consumption) used during nitridization and for further growth of $Al_xGa_{1-x}N$/AlN heterostructures corresponded to the GaN equivalent growth rate in the order of $0.05\,\mu$m/h.

Epitaxial synthesis of heterostructures began with the formation of AlN nucleus layers on the substrate surfaces at $T \sim 800°C$, $F_{Al} \sim 0.02\,\mu$m/h grown for 60 min. Then the temperature of the substrates dropped to $T \sim 700°C$ for the growing $Al_xGa_{1-x}N$ base layer during 4 h at constant values $F_{Al} \sim 0.01\,\mu$m/h, $F_{Ga} \sim 0.4\,\mu$m/h and $F_N \sim 0.04-0.05\,\mu$m/h. It should be noted that a gradual increase of the pyrometer temperature to $T \sim 707°C$ was observed during the growth process.

Structural studies of the samples were performed using high-resolution X-ray diffraction with Bruker D8 Discover diffractometer in parallel beam mode with linear focusing. The primary X-ray beam of the copper tube is monochromatized using a Ge220 crystal with double reflection.

Libra 120 Carl Zeiss electron microscope was used for microscopic studies of heterointerfaces while surface morphology features were studied using a Femtoscan-001 NT MDT scanning probe microscope.

The surface layer chemical state data were studied by X-ray photoelectron spectroscopy (XPS). The spectra were recorded by the SPECS spectrometer (Germany). Excitation using Mg K_α-radiation ($E = 1253.6$ eV). Sample surfaces were irradiated with ions Ar^+ with an energy of 4 keV and an electron current density $10\,\mu A/cm^2$ at a layer removal rate of ~ 1 nm/min for removal of possible contamination from them.

The optical properties of the samples were studied in the range 190–900 nm by ultraviolet (UV) spectroscopy using Perkin Elmer LAMBDA 650 spectrophotometer with Universal Reflectance Accessory (URA), which allows obtaining reflection spectra in the range of angles of incidence from 8 to 80°.

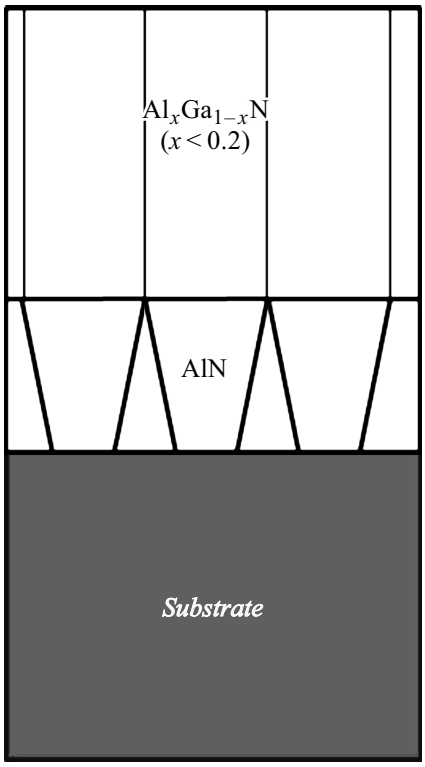

Figure 1. Schematic illustration of the studied heterostructures with different types of substrates (*c*-Si, por-Si and SiC/por-Si/*c*-Si).

The luminescence spectra of the samples were studied using Accent RPM Sigma photoluminescence and optical reflection measurement tool. The studies were carried out at room temperature with excitation by 266 nm laser, $W = 5\,W/cm^2$.

2. Results and discussion

The microstructure and surface morphology of $Al_xGa_{1-x}N$/AlN heterostructures grown on different types of substrates were studied by scanning electron microscopy (SEM) and atomic force (AFM) microscopy, respectively.

Fig. 2 shows SEM images of the sample cleavage. These images show that all films have a nanocolumn morphology, their thickness varies, and it depends on the type of substrate used. In addition, it was found that the thickness of the grown heterostructures was slightly below the growth process specifications. For instance, the total thickness of $Al_xGa_{1-x}N$/AlN heterostructure on *c*-Si and por-Si/*c*-Si substrates was ~ 92 and ~ 94 nm, respectively, while the thickness of $Al_xGa_{1-x}N$/AlN heterostructures together with the SiC layer on SiC/por-Si/*c*-Si hybrid substrate reached ~ 140 nm: ~ 30 nm — solid SiC layer, ~ 106 nm — nanocolumnar AlGaN/AlN heterostructure.

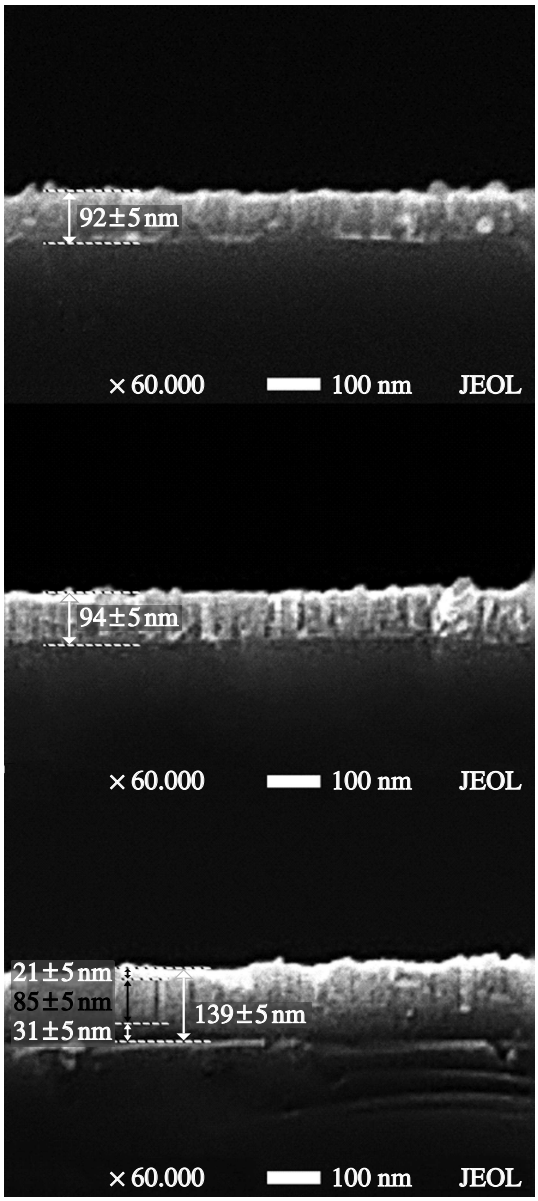

Figure 2. SEM images of cleavage of $Al_xGa_{1-x}N$/AlN heterostructures grown on various substrates: *a* — *c*-Si; *b* — por-Si/*c*-Si; *c* — SiC/por-Si/*c*-Si.

It is noteworthy that not only the thickness of the layers, but also the surface morphology of $Al_xGa_{1-x}N$/AlN heterostructures turned out to depend on the type of substrate used. Fig. 3 shows typical images of film surface areas.

The AFM image analysis shows that the surface of the sample grown on *c*-Si substrate is characterized by a comb structure. In turn, the ridges have a fine-grained structure, the grain size varies in a wide range from several tens to one hundred nanometers. Clusters with a diameter of 100 to 200 nm consisting of smaller globules are observed on the surface. The height of the globules is 50−60 nm. The surface of the por-Si/*c*-Si sample also has a comb structure. The ridges, as well as in the case of the sample *c*-Si, have a fine-grained structure. There are dome-shaped clusters on the ridges with a diameter from 100 to 150 nm and an average height of 55−60 nm.

It is noteworthy that the nanocolumns of the heterostructure grown on a hybrid SiC/por-Si/*c*-Si substrate were the most densely packed. The surface of this heterostructure had the smoothest morphology, characterized by the absence of ridges and clusters and had a fine-grained structure. The diameter of the grains, which are evenly distributed over the entire surface of the sample, ranges from 30 to 60 nm.

The use of AFM in semi-contact mode and the use of specialized software made it possible to evaluate the surface roughness of heterostructures. The surface roughness of heterostructures of samples grown on *c*-Si, por-Si/*c*-Si and SiC/por-Si/*c*-Si substrates was 5.4, 5.8 and 6.3 nm, respectively. Therefore, AFM data indicate that there are no larger-scale „globules“ and „clusters“ on the surface in the case of the $Al_xGa_{1-x}N$/AlN heterostructure grown on SiC/por-Si/*c*-Si substrate. This is also evidenced by the cross-section profiles of the surface of the sections (Fig. 3).

The reasons for small differences of the thicknesses of the layers of $Al_xGa_{1-x}N$/AlN heterostructures observed in the SEM images will be discussed below.

It is known from the literature that the thermal stability of $Al_xGa_{1-x}N$ layers, even with a relatively high content of Al ($x \sim 0.5$), is determined by a less strong bond Ga−N. As in the case of GaN growth, a higher rate of GaN decomposition, resulting in a high rate of Ga and N adatom desorption, is observed for the metal-polar surface of $Al_xGa_{1-x}N$ layer at $T > 680^\circ$C. N-polar GaN layers decompose at higher temperatures, namely at $T > 750^\circ$C [20]. We studied the polarity of the grown heterostructures to confirm these processes. All samples had a granular morphology before etching according to the results obtained (Fig. 2). After etching in KOH, small islands of Al(Ga)N were observed on the surface, which were formed as a result of thinning of areas close to the base of the columns/grains, which was observed earlier in [21,22]. The formation of a characteristic pyramid-shaped relief on the upper edges of the grains was not observed. This fact indicates that epitaxial growth in the N-enriched environment results in the formation of $Al_xGa_{1-x}N$/AlN heterostructures with a Ga-polar surface.

The chemical composition of the surface of $Al_xGa_{1-x}N$ solid solution in heterostructures grown on *c*-Si, por-Si/*c*-Si and SiC/por-Si/*c*-Si substrates was studied using X-ray photoelectron spectroscopy (XPS, XPS). When calculating the concentrations of Ga and Al atoms in $Al_xGa_{1-x}N$ solid solution, we proceeded from the ratio of the integral intensities of N−Ga and N−Al bonds according to the results of simulation of XPS spectra N1*s* in the Casa XPS software product. The results are shown in the Table 1.

According to the results obtained $Al_xGa_{1-x}N$ solid solution with $x \sim 0.2 \sim F_{Al}/F_N$ was formed only on SiC/por-Si/*c*-Si hybrid substrate, while $Al_xGa_{1-x}N$ layer was not formed on *c*-Si- and por-Si/*c*-Si substrates, only GaN layer with a small impurity AlN is detected (with $x < 0.07$).

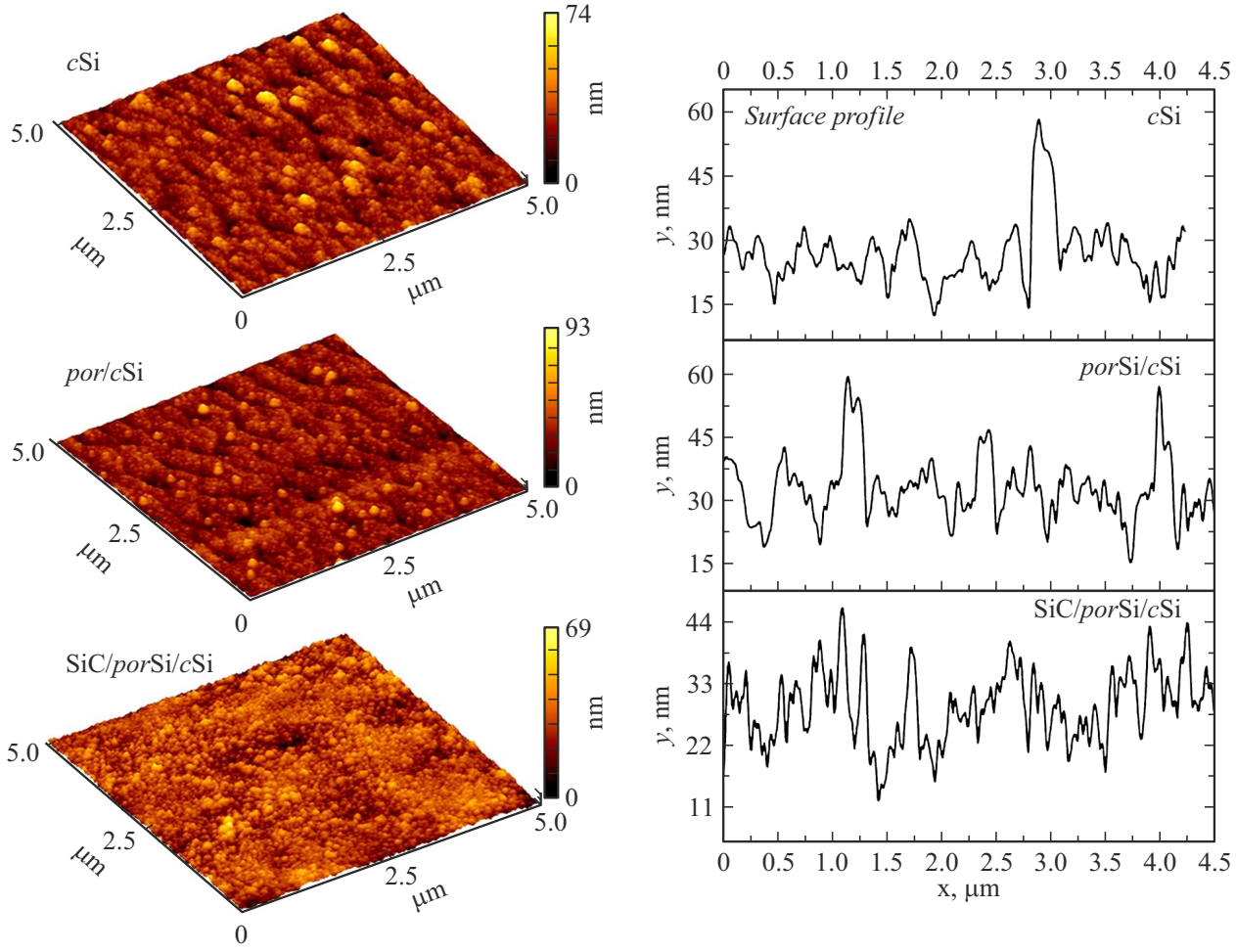

Figure 3. Typical AFM images of surface areas $5 \times 5\,\mu$m (left) and surface cross-section profiles of $Al_xGa_{1-x}N$/AlN heterostructures grown on three types of substrates.

Table 1. Integral intensities of N−Ga and N−Al bonds and calculated concentrations of Ga and Al in solid solution $Al_xGa_{1-x}N$

Sample	C_{Ga}, %	C_{Al}, %
c-Si	∼ 94.1	∼ 5.0
por-Si/*c*-Si	∼ 93.1	∼ 6.9
SiC/por-Si/*c*-Si	∼ 81.5	∼ 18.5

Fig. 2, *a* and *b* shows that this layer is quite loose and, as noted above, consists of loosely adjacent nanocolumns. Naturally, the mechanisms of AlGaN growth on *c*-Si and por-Si/*c*-Si substrates differ from the mechanism of AlGaN growth on the SiC/por-Si/*c*-Si substrate. The development of a quantitative model requires separate consideration, which will be done in the future. We will try to explain the difference of the mechanisms of AlGaN formation on *c*-Si, por-Si/*c*-Si and SiC/por-Si/*c*-Si substrates so far only at a qualitative level in this study. First of all, we would like to note that the difference of the parameters of GaN and Si lattices is 14.8%, while this difference between AlN and Si reaches 19%. There is also a difference between the linear coefficients of thermal expansion of the lattices. Therefore, the linear coefficients of GaN and Si thermal expansion differ by 33% at room temperature. The 3C-SiC layer also acts as a compensating buffer, reducing elastic stresses in heteroepitaxial layers of III−N. Coating silicon with a 3C-CiC layer on Si makes it possible to overcome not only the difference of the parameters of the AlN and Si lattices, but also the difference of the values of thermal linear expansion coefficients (TLEC). For instance, the TLEC of a hexagonal GaN along the axis *a* is $\alpha^{GaN} \approx 4.9 \cdot 10^{-6}\,K^{-1}$ at a temperature of 700 K and this coefficient has the value of $\alpha^{GaN} \approx 3.9 \cdot 10^{-6}\,K^{-1}$ at a temperature of 300 K, according to the database of the Ioffe Physical-Technical Institute [23]; TLEC of hexagonal AlN along the axis *a* is $\alpha^{AlN} \approx 4.2 \cdot 10^{-6}\,K^{-1}$ at a temperature of 300 K, and it is equal to $\alpha^{AlN} \approx 5.9 \cdot 10^{-6}\,K^{-1}$ at a temperature of 700 K. TLEC of 3C-SiC is approximately equal to $4.4 \cdot 10^{-6}\,K^{-1}$ at $T = 700$ K, according to [24],while TLEC 3C-SiC is approx-

imately equal to $3.8 \cdot 10^{-6}\,K^{-1}$ at a temperature of 300 K according to [23]. TLEC of silicon is $2.6 \cdot 10^{-6}\,K^{-1}$ [24] at a temperature of 300 K and at $T = 700$ K TLEC of silicon is in the order $3.8 \cdot 10^{-6}\,K^{-1}$. These data should be treated with a certain degree of caution. The fact is that bulk single crystals of GaN are a rather rare material, and bulk crystals of 3C-SiC practically do not exist at all, unlike hexagonal crystals of SiC. Usually 3C-SiC samples are thin-film objects on foreign substrates, so the exact determination of TLEC is quite a difficult task. Still these data show that coating of Si with a 3C-SiC layer reduces the difference of TLEC. So, the difference between TLEC of Si and AlN is in the order of 38% at room temperature, and the difference between TLEC of 3C-SiC and AlN is in the order of 9.5%. It should be noted that the linear coefficients of thermal expansion should depend on the substrate structure, i.e.the TLEC of *c*-Si and TLEC por-Si/*c*-Si should be different. Obviously, these coefficients for por-Si/*c*-Si will depend on both the pore density and their size. This issue, however, requires a separate study.

Now let's consider the structural features of SiC films grown on Si by the method of coordinated atomic substitution. Every fifth cell of SiC is almost coherently conjugated with every fourth cell of Si in the process of conversion of Si to SiC according to [25]. At the same time, the remaining bonds at the interface between SiC and Si are broken, and pores form under the SiC layer in these places. The distance between atoms C along the plane (111) in projection onto the plane $(11\bar{2})$ in SiC is 3.08 Å [25]. The similar distance between Si atoms in silicon is 3.84 Å. It follows that the distance between the planes of the five cells in SiC = 15.40 Å, and the distance between the four cells Si = 15.36 Å. Consequently, it is no longer the SiC film that has a smaller lattice parameter size relative to the original silicon substrate, but, on the contrary, the „new" substrate (four silicon cells with pores under their surface) has a smaller lattice parameter at the interface points. Thus, in this case, the substrate compresses the SiC film. The deformation resulting from the difference between these parameters is insignificant and amounts to 0.3%. A similar effect, as shown in [25,26], results in a significant change of the growth mechanisms of various films on SiC/Si compared with the growth of films on Si. A porous layer is formed in Si between the SiC and Si layer in the process of conversion of Si to SiC, the pores of this layer are covered with SiC from the inside. Actually, this can be seen in Fig. 2, *c*. In our case, the SiC layer was previously synthesized on the pore-coated surface of the Si. It should be noted that SiC growth processes on porous Si were studied in in [27] under various synthesis conditions. At the same time, the growth of SiC was studied by the method of substitution of atoms on Si, covered with an ensemble of two types of pores, namely large ones with a diameter of ~ 500 nm and small ones with a diameter of ~ 17 nm. The results showed that the structural properties of the grown SiC layer practically did not differ from the SiC layer grown on nonporous Si during the synthesis of SiC on Si coated with an ensemble of small pores, and they are what we are interested in this case. However, at the same time, this layer had a very important and distinctive property from the SiC layer grown on nonporous Si: it could easily be separated from the surface Si, i.e. this layer has only minor contact with Si. It was shown in the same work ([27]) that the presence of a porous SiC buffer layer results in a significant decrease of mechanical stresses caused by the difference of TLEC.

The following conclusions can be drawn based on these data regarding the reasons for such a striking difference in the structure of AlGaN layers grown on *c*-Si, por-Si/*c*-Si and SiC/por-Si/*c*-Si substrates. Large elastic stresses occur on *c*-Si substrate during the deposition of AlGaN, caused by both a large difference of the lattice parameters of these substances and a large difference of their TLEC. This results in a change of the equilibrium concentrations of Al, Ga and N adatoms, from which AlGaN nuclei are formed by $x\mathrm{Al} + (1-x)\mathrm{Ga} = \mathrm{Al}_x\mathrm{Ga}_{1-x}\mathrm{N}$ type reaction. As is known, the rate of stationary nucleation of nuclei of a new phase is determined by the Boltzmann distribution $I = K\exp(-\Delta F^*/kT)$ [28], where ΔF^* — free energy of formation of a critical-sized nucleus, K — pre-exponential multiplier depending on the kinetic parameters of nucleus growth. The free energy of the formation of AlN, GaN and AlGaN, ΔF^* according to [28] depends on the equilibrium constants of the chemical reactions of the formation of these substances occurring on the surface of the substrates. Both the equilibrium concentrations of Al, Ga and N adatoms and the formation of the nuclei themselves will change under the impact of elastic energy. As a result, the reaction rate of AlGaN formation may be lower than the reaction rate of aluminum nitride formation $\mathrm{Al} + \mathrm{N} = \mathrm{AlN}$ or the reaction rate of formation of pure $\mathrm{Ga} + \mathrm{N} = \mathrm{GaN}$. As a result, their nucleation rate will be lower. That is why, in our opinion, AlGaN is not formed on the substrate *c*-Si. The por-Si/*c*-Si substrate is preferable in this sense. As we discussed above, pores lead to relaxation of thermal stresses. Obviously, the probability of an AlGaN formation reaction increases although slightly, which ultimately results in an increase of the probability of its nucleation. However, the presence of pores can result in the uneven distribution of both thermal elastic stresses and elastic stresses caused by differences of lattice parameters over the entire surface of the substrate. These stresses above the pores can be reduced to zero, and they will reach high values on a pore-free surface. This will result in the uneven formation of the AlGaN layer both in terms of composition and structure. If we take into account the fact that the inner part of the pores can be filled with various gases and, especially, water vapor, which are very difficult to desorb even at high temperatures, AlGaN will not grow plastically on this substrate either, since water vapor will prevent the nucleation of the epitaxial structure in this case.

The pore layer is covered with a SiC layer on the surface of the SiC/por-Si/*c*-Si substrate, the parameters of the SiC and AlGaN lattices slightly differ. As we have shown

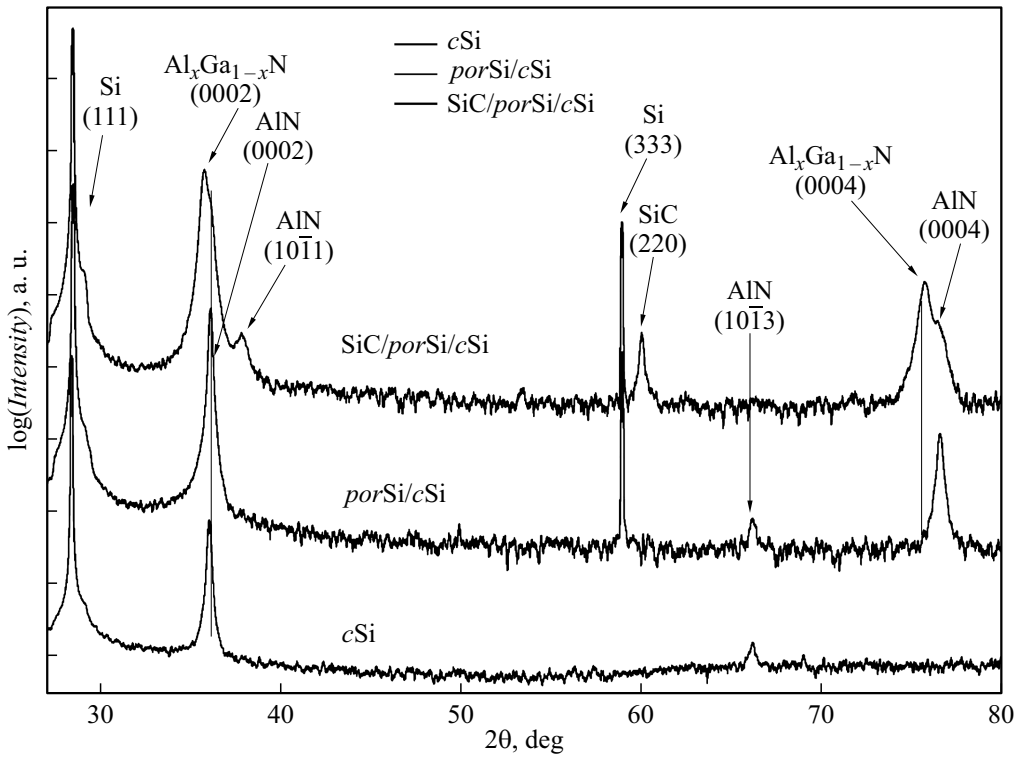

Figure 4. X-ray $\omega/2\theta$ diffraction for samples of $Al_xGa_{1-x}N$/AlN heterostructures grown on various substrates.

above, the TLEC coefficients are also close. Numerical calculations were performed using the example of GaN growth on a SiC/por-Si substrate in [27]. They showed that the presence of pores under the SiC layer results in the periodic modulation of mechanical stresses, while SiC films lying directly at Si have no mechanical stresses. Calculations also showed that mechanical stresses can reach significant values directly in the contact zone of the buffer layer and the GaN film, but they decrease very quickly with the increase of the film thickness. It turned out that an increase of pore depth results in a decrease of elastic thermal stresses. Therefore, the presence of such a pore system helps to significantly reduce the mechanical stresses on the surface of the thin film resulting from differences of TLEC.

Therefore, our experimental studies clearly showed that a large difference of the substrate–film lattice parameters result not only in the occurrence of various kinds of defects, but also significantly affects the chemistry of solid solution formation, in this case, the chemistry of AlGaN formation, and SiC substrates grown on porous Si to overcome this negative trend.

X-ray $\omega/2\theta$ scans were performed to study the phase composition and crystal structure of the samples, the scan images are shown in Fig.4. The analysis shows that the diffraction reflection belonging to the (111) plane of a monocrystalline silicon substrate is the main and most intense diffraction reflection. Moreover, a low-intensity reflex (333) forbidden for Si appears on $\omega/2\theta$ diffractograms of samples containing por-Si layers, which, apparently, is a consequence of a disruption of the symmetry of the crystal lattice in the porous layer.

As for the diffraction from the epitaxial film $Al_xGa_{1-x}N$/AlN, its intensity is 3–4 orders of magnitude lower than diffraction from Si substrate, and indicates a small thickness of the epitaxial layer. According to the experiment, the diffraction patterns of all $Al_xGa_{1-x}N$/AlN heterostructures show maxima around 36.05, 37.9, 66.11 and 76.5°, which belong to reflections from the planes (0002), (10$\bar{1}$1), (10$\bar{1}$3) and (0004) wurtzite AlN. Reflexes 0002 and 0004 are the most intense in this set, which indicates that the AlN columns are predominantly grown along the ⟨0001⟩ direction in all three samples. However, the presence of additional low-intensity reflections on the diffractograms (10$\bar{1}$1) and (10$\bar{1}$3) indicates both the misorientation of the AlN nanocolumns relative to the growth direction given by the (111) orientation of the Si substrate, and the probable overgrowth of the AlN nanocolumns in the direction of ⟨10$\bar{1}$1⟩ and ⟨10$\bar{1}$3⟩, which correlates with the results we have already demonstrated for ultrathin nanocolumns GaN [15].

It should be noted that a reflex of about 35.8° is observed only on the diffractogram of a sample grown on a SiC/por-Si/*c*-Si substrate, which can be strictly attributed to (0002) reflection from $Al_xGa_{1-x}N$ solid solution. In addition, the $\omega/2\theta$ diffraction pattern of the SiC/por-Si/*c*-Si sample has a diffraction maximum attributed to the cubic polytype SiC-3C, because (111) SiC faces are always formed on the S surface regardless of orientation of Si, processing of Si, or

Table 2. Results of X-ray diffractometry

Sample	Layer	*c*-parameter lattices, Å	*a*-parameter lattices, Å	Stress in *c*-direction, ε_{zz}	Stress in *a*-direction, ε_{xx}	Biaxial Stress in the plane σ_{xx}, GPa
SiC/por-Si/*c*-Si	AlGaN	5.1144	3.21237	−0.0054	0.0110	5.27
	AlN	4.9784	3.111937	$-2.25 \cdot 10^{-4}$	$4.17 \cdot 10^{-4}$	0.20
por-Si/*c*-Si	AlGaN	–	–	–	–	–
	AlN	4.9735	3.1179	−0.0011	0.0023	1.12
c-Si	AlGaN	–	–	–	–	–
	AlN	4.9728	3.1187	−0.0013	0.0026	1.27

formation of pores in Si, due to the peculiarities of the mechanism of coordinated substitution of [11] atoms, as shown in [27]. (111) SiC faces can be tilted or rotated relative to the (111) Si face at the interface of pores and (111) Si surface.

It should be noted that the absence of reflections from $Al_xGa_{1-x}N$ on diffractograms of *c*-Si and por-Si/*c*-Si samples is attributable to the different efficiency of embedding Ga atoms in the epitaxial synthesis of AlGaN solid solutions on a nanocolumnar buffer layer of AlN grown on silicon substrates without a SiC layer and with this layer. The differences of the thicknesses of the layers of heterostructures $Al_xGa_{1-x}N$/AlN observed in SEM images confirm the formation of Ga-enriched clusters with a crystal structure that has no long-range order, which most likely results in the blurring of the AlGaN diffraction reflexes for *c*-Si and por-Si/*c*-Si structures.

Based on X-ray diffraction data, the lattice parameters of AlN epitaxial layer of and $Al_xGa_{1-x}N$ solid solution were calculated within the framework of the approach described in [15]. In accordance with the anisotropic theory of elasticity, planar deformation ε_{xx} (along the axis a) and out-of-plane deformation ε_{zz} (along the axis c are determined for epitaxial layers with a wurtzite lattice), and also biaxial stresses in the plane of growth (the in-plane biaxial stress) σ_{xx} [29]. It was assumed that the use of Poisson's−Vegard's law is valid for calculating the parameters of the crystal lattice, as well as the elastic deformation coefficients $C(x)_{ij}$ for solid solutions, [30–34].

The calculated values of the crystal lattice constants, the strain components in plane ε_{xx} and in the direction of growth ε_{zz}, as well as stresses in the plane of growth σ_{xx} for the epitaxial layers of the studied samples are listed in Table 2.

The obtained results show that the strains in AlN and $Al_xGa_{1-x}N$ layers have different signs. They are tensile in the plane of growth, they are compressive in the direction of growth. This is due to the discrepancy between the parameters of the crystal lattices of the substrate and the epitaxial layers AlN and $Al_xGa_{1-x}N$. It should be noted that the lowest level of residual stresses σ_{xx} for the AlN layer is observed in a sample formed on SiC/por-Si/*c*-Si hybrid substrate. However, the level of residual stresses σ_{xx} in a layer of $Al_xGa_{1-x}N$ solid solution of a heterostructure grown on a SiC/por-Si/*c*-Si substrate is an order of magnitude higher than the level of residual stresses observed in AlN sublayer.

The crystal quality of the grown $Al_xGa_{1-x}N$/AlN heterostructures was characterized by measurements of X-ray rocking curves. ω-diffraction curves near (0002) AlN node are shown in Fig. 5.

A preliminary analysis of the ω rocking curves (Fig. 5) showed that the curve profile of the heterostructure grown on a SiC/por-Si/*c*-Si substrate has a noticeable asymmetry. This fact is associated with the overlap of reflexes from different layers of the heterostructure taking into account the data of $\omega/2\theta$ scans. The profile was deconvoluted into components to determine the contributions of each maximum (Fig. 5, right). Origin 8 program was used for simulation. The number of extremums was determined using the second derivative. It is clearly seen that the shape of the profile is attributable to the superimposition of a line from the AlN layer and $Al_xGa_{1-x}N$ solid solution, as well as a low-intensity maximum located at large diffraction angles. This reflex belongs to the cubic 3C-SiC with a lattice that has tetragonal distortions because of mismatch of the crystal lattice parameters.

The angular range of disorientation of the crystallites in the epitaxial film can be estimated as the difference between the width of the swing curve of the layer ω^f_{RC} and the instrumental width ω^i_{RC} since the angular width of the reflex on the ω rocking curve correlates with the mosaic (reversal angle) of the crystallites relative to each other. The width of 004 reflex of the NIST SRM silicon standard, measured under similar conditions, is taken as the instrumental width $\omega^i_{RC} = 0.014°$.

The results show that the η mosaicity of the AlN layer has the values ± 0.62, ± 0.55 and $\pm 0.67°$ for samples grown on *c*-Si, SiC/*c*-Si and SiC/por-Si/*c*-Si substrates. It is clearly seen that a lower dispersion of mosaicity is characteristic of the nanocolumnar epitaxial structure grown on a por-Si/*c*-Si substrate, which we have already observed earlier, but for thick layers [14,35]. At the same time, the mosaicity value of nanocrystals of $Al_xGa_{1-x}N$ solid solution grown on SiC/por-

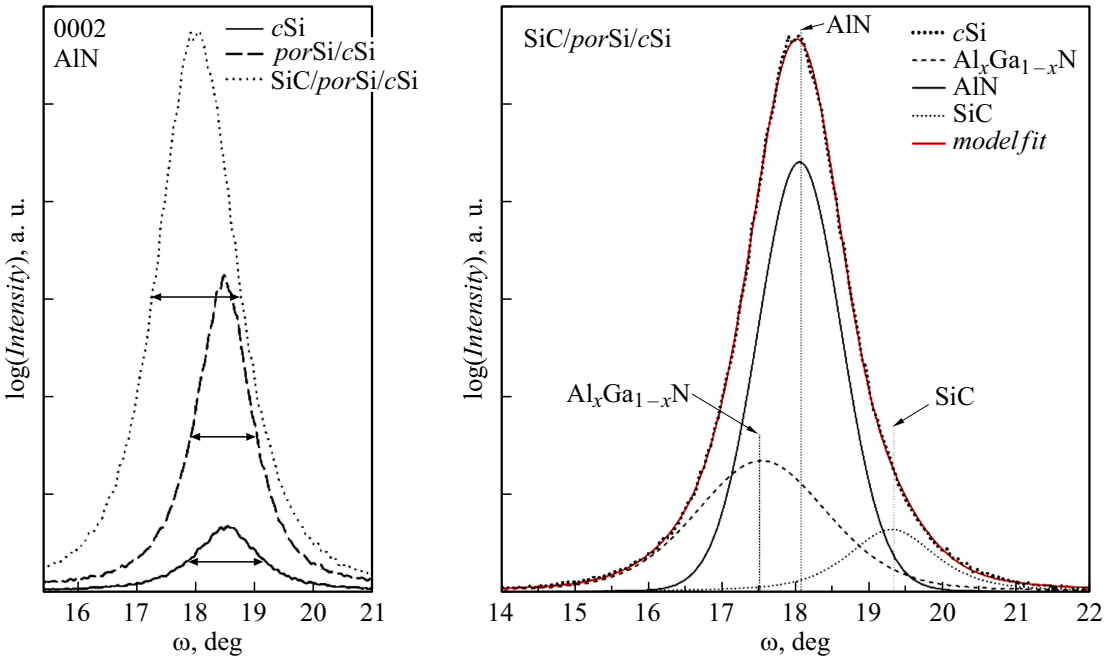

Figure 5. X-ray ω-rocking curves near the 0002 AlN plane for c-Si, por-Si/c-Si and SiC/por-Si/c-Si samples (on the left). The deconvolution of the rock curve near 0002 AlN plane for SiC/por-Si/c-Si sample (right).

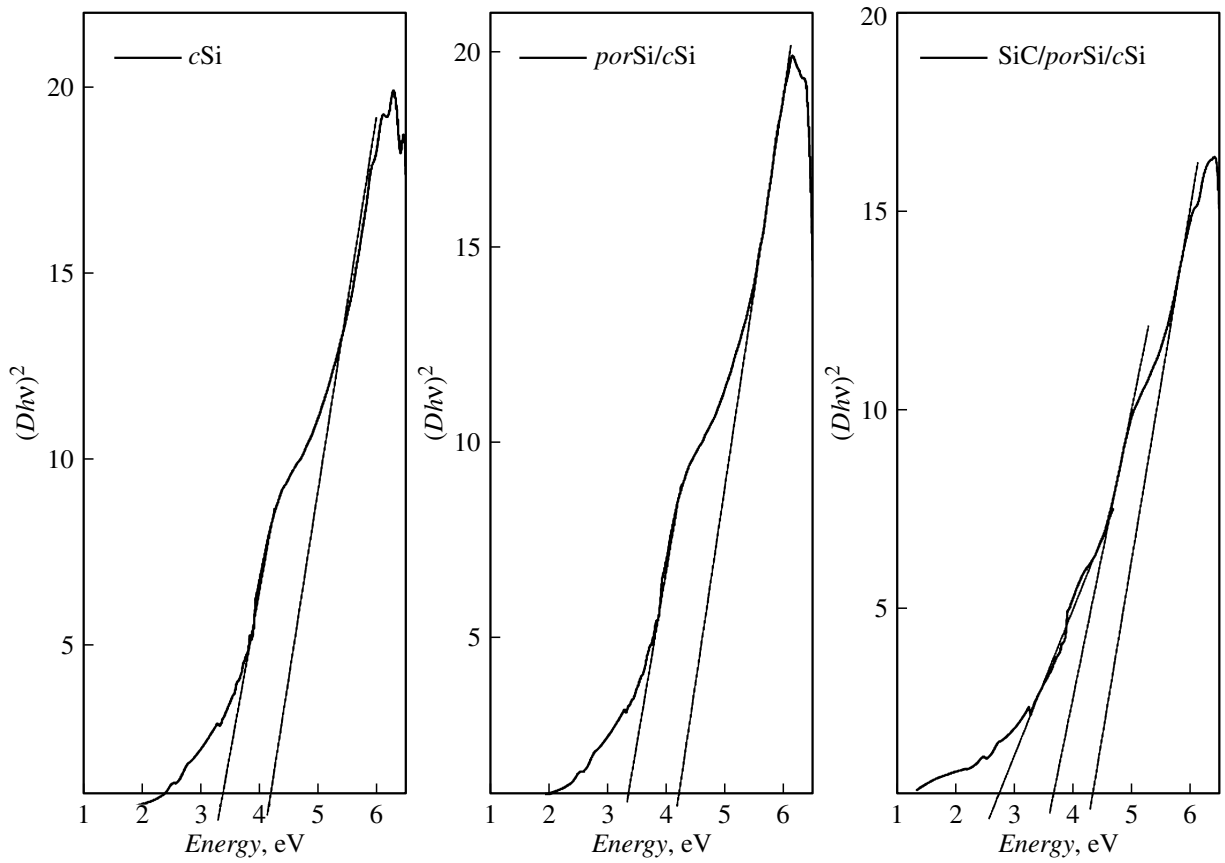

Figure 6. Graphical analysis by the Tautz method of dependencies $(D \cdot h\,nu)^2$ on optical radiation energy for heterostructures $Al_xGa_{1-x}N$/AlN grown on substrates c-Si (left), por-Si/c-Si (center) and SiC/por-Si/c-Si (right).

Si/*c*-Si is ± 1.02. The increase of the FWHM of the X-ray ω-rocking curve is explained by the slope of the nanocolumns caused by stress relaxation of the mismatch between the parameters of the epilayer lattices and the substrate.

The optical properties of $Al_xGa_{1-x}N$/AlN heterostructures in the UV wavelength region were studied on the basis of the methodology used in a number of studies [36]. Transmission spectra of −reflections were obtained for this purpose in the 1−6 eV region and were used to calculate the optical density D. The dependencies $(D \cdot h\nu)^2$ on $h\nu$ were constructed after that and their graphical analysis was performed by the Tautz method [37,38]. As a result, areas with a linear dependence $(D \cdot h\nu)^2$ were found, indicating the presence of direct resolved transitions in this spectral region, the energies of which were compared with known literature data of similar samples.

It follows from the results obtained (Fig. 6) that the occurrence of two direct transitions with energies in the ranges of 3.2−3.6 eV and 4.1−4.4 eV is characteristic in all the studied samples. At the same time, another transition was detected in the region of lower energies ~ 2.5 eV for a heterostructure grown on a SiC/por-Si/*c*-Si substrate using the Tautz method (Fig. 6, right).

The observed high-energy transition can be attributed to a direct resolved band-to-band transition of the band−band type at point Γ of the Brillouin zone in the wurtzite AlN and coinciding with the energy width of its band gap.

Despite the fact that a large number of literature sources indicate that the band gap width AlN $E_g \sim 6$ eV, the phenomenon of narrowing of the band gap to a value of $E_g \sim 4.1$ eV in aluminum nitride films grown at reduced substrate temperatures has been repeatedly demonstrated [39]. There are also known studies that demonstrated the value of $E_g \sim 5.1$ eV for AlN films grown on Si(100) substrates at various substrate temperatures: from room temperature (RT) to 500°C [40]. A narrowing of the AlN band gap to $E_g \sim 4.6$ eV was also observed in films of highly textured aluminum nitride [41]. The second transition found in all structures near 3.2−3.6 eV, is probably associated with a high density of defects in the material, which form levels in the band gap and density tails of states in the valence band and conduction band.

As for the direct transition ~ 2.5 eV, detected in a sample grown on a SiC/por-Si/*c*-Si substrate, then this absorption band coincides well with the energy of the band gap of the cubic polytype of silicon carbide 3C-SiC E_g $(\Gamma 15v - X1c) \sim 2.41$ eV [42]. At the same time, it was noted in [43] that deformations occurring in thin layers can cause a sufficiently large (up to 0.5 eV) shift in the magnitude of the optical band gap. Considering the fact that the error of the method we used to study optical properties is $\sim 0.1-0.2$ eV, the direct transitions experimentally detected in 3.95−4.15 eV region can quite possibly be correlated with optical absorption from $Al_xGa_{1-x}N$.

It should be noted that the experimentally detected shifts in the energies of direct transitions for GaN correlate with the value of the biaxial stress in the plane σ_{xx} calculated using the X-ray diffractometry data.

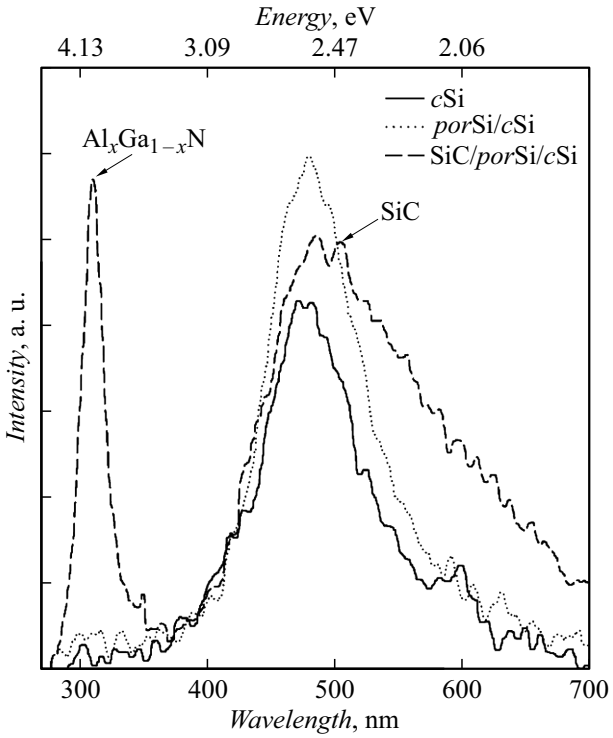

Figure 7. PL spectra at $T \sim 300$°C from $Al_xGa_{1-x}N$/AlN heterostructures grown on *c*-Si, por-Si/*c*-Si and SiC/por-Si/*c*-Si substrates.

Fig. 7 shows photoluminescence spectra of epitaxial heterostructures $Al_xGa_{1-x}N$/AlN of all studied samples. It is clear that the luminescence of the samples in 300−900 nm region depends on the type of substrate used for growth.

Studies show that a high-energy peak with a maximum energy of $E_g = 3.99$ eV, i.e. in the UV spectral region near 310 nm, is present only in the FL spectrum of $Al_xGa_{1-x}N$/AlN heterostructure, grown on a SiC/por-Si/*c*-Si substrate. Moreover, a broad additional yellow band can be observed in the spectra of all the studied samples, which, as a rule, is associated with the presence of deep defects in $A_{III}N$ layers [44].

It should be noted that there is a peak with a maximum of about 2.34 eV in the PL spectrum of the sample grown on a hybrid SiC/por-Si/*c*-Si substrate. This peak can be attributed to the 3C-SiC sublayer, for which the band gap is $E_g \sim 2.24-2.39$ eV [45,46], which also correlates with our results obtained using the UV method.

It is known that the value of the optical band gap can be used to evaluate the composition of $Al_xGa_{1-x}N$ solid solution [47].

The dependence of the band gap energy on the Al content is nonlinear in $Al_xGa_{1-x}N$ solid solution according to Vegard's law:

$$E_g^{Al_xGa_{1-x}N}(x) = E_g^{GaN}(1-x) + E_g^{AlN}x - bx(1-x), \quad (1)$$

where b — bending parameter ($\sim 1.0 \pm 0.3$ at room temperature), $E_g^{\mathrm{GaN}} = 3.45\,\mathrm{eV}$, $E_g^{\mathrm{AlN}} = 6.13\,\mathrm{eV}$. However, the last term in (1) can be neglected for $x \leq 0.25$ and the dependence is linear was shown in [48].

Taking into account these assumptions, the composition of $Al_{0.20}Ga_{0.80}N$ solid solution was determined for the heterostructure grown on a SiC/por-Si/c-Si substrate, which is in excellent agreement with the results of photoelectron microscopy. The fact that we do not observe UV PL from samples grown on por-Si/c-Si and c-Si substrates also correlates with the results of X-ray diffraction, indicating the absence of a formed $Al_{0.2}Ga_{0.8}N$ solid solution in these samples.

3. Discussion

Combining the methods of structural, microscopic and spectroscopic diagnostics, we conducted comparative studies of nanoscale columnar $Al_xGa_{1-x}N$/AlN heterostructures synthesized on c-Si, por-Si/c-Si, and SiC/por-Si/c-Si by the PA MBE.

According to the experimental data, the composition, thickness and morphology of the deposited film, as well as the aluminum content in $Al_xGa_{1-x}N$ solid solution depend on the type of substrates used in this work. $Al_xGa_{1-x}N$ layer with the composition $x \sim 0.20$ was formed only on a hybrid SiC/por-Si/c-Si substrate, while AlGaN layer was not formed on c-Si and por-Si/c-Si substrates. It was found that the epitaxial growth of $Al_xGa_{1-x}N$ heterostructures in the N-enriched environment resulted in the formation of $Al_xGa_{1-x}N$/AlN layers with a Ga-polar surface.

The analysis of microscopy data also confirms the formation of a layer with nanocolumnar morphology, while the lateral size of grains (nanocolumns) varies in a wide range from several dozens to one hundred nanometers. The formed $Al_xGa_{1-x}N$ nanocolumns have a slope relative to the c-axis, which is apparently caused by the relaxation of elastic stresses of the mismatch of the parameters of the lattices of the epi-layer and substrate.

As for the optical properties of the samples of $Al_xGa_{1-x}N$/AlN heterostructures in $1-6\,\mathrm{eV}$ region, the optical absorption/luminescence of the samples also depends on the type of substrate used for growth. It is shown that a high-energy peak with energy $E_g = 3.99\,\mathrm{eV}$ corresponding to the value of the band gap of $Al_xGa_{1-x}N$ solid solution ($x \sim 0.2$) is observed only in the PL spectrum of the $Al_xGa_{1-x}N$/AlN heterostructure grown on a SiC/por-Si/c-Si substrate. At the same time, a yellow photoluminescence band is observed in the spectra of all studied samples, which, as a rule, is associated with the presence of deep defects in $A_{III}N$ layers [49].

Therefore, studies showed that under the same PA MBE conditions $Al_xGa_{1-x}N(x \sim 0.2)$/AlN heterostructure with nanocolumnar morphology grows satisfactorily on SiC/por-Si/c-Si hybrid substrate, and $Al_xGa_{1-x}N$ layer with a smaller $x < 0.07$ on c-Si and por-Si/c-Si substrates is only in the disordered solid solution stage.

The obtained results clearly indicate different mechanisms of growth of $Al_xGa_{1-x}N$ films on a nanocolumnar buffer layer of AlN grown on silicon substrates without and with a SiC layer. The presence of a SiC layer grown on porous Si in the template effectively affects the mechanisms of film growth and its adsorption characteristics, increasing the nucleation rate of ordered solid solution of $Al_xGa_{1-x}N$ of a given composition and, as a result, affects the structural and optical qualities of $A_{III}N$ structures.

The results presented in this paper demonstrate the potential of using SiC/por-Si/c-Si substrates for the integration of silicon technology and the technology of synthesis of nanoscale columnar $Al_xGa_{1-x}N$ heterostructures by molecular beam epitaxy with plasma activation of nitrogen.

Funding

A.S. Lenshin performed microscopic studies and obtained data on the chemical state of the layers with the financial support of a grant from the Russian Science Foundation 19-72-10007.
P.V. Seredin, D.L. Goloshchapov and D.N. Nesterov performed structural spectroscopic studies with the support of a grant from the Ministry of Science and Higher Education of the Russian Federation (grant no. FZGU-2023-0006).
S.A. Kukushkin synthesized the SiC/Si substrate and carried out a theoretical analysis of the growth process of AlGaN layers in within the framework of the state assignment of the Ministry of Science and Higher Education of the Russian Federation at FGPU IPMash RAS. Contract no. FFNF-2021-0001, subject no. 121112500383-9.
A.M. Mizerov, M.S. Sobolev, S.N. Timoshnev and K.Y. Shubina carried out the growth of AlGaN structures using the MPE PA method and conducted studies of their polarity within the framework of State Task No. FSRM-2023-0006. In terms of access to scientific equipment and methodology, this study was supported by The Ministry of Education and Science of the Russian Federation under the agreement No. 075-15-2021-1351.

Conflict of interest

The authors declare that they have no conflict of interest.

References

[1] G. Dewey, M.K. Hudait, Kangho Lee, R. Pillarisetty, W. Rachmady, M. Radosavljevic, T. Rakshit, R. Chau. IEEE Electron Device Lett., **29**, 1094 (2008). DOI: 10.1109/LED.2008.2002945
[2] D. Kohen, X.S. Nguyen, S. Yadav, A. Kumar, R.I. Made, C. Heidelberger, X. Gong, K.H. Lee, K.E.K. Lee, Y.C. Yeo, S.F. Yoon, E.A. Fitzgerald. AIP Adv., **6**, 085106 (2016). DOI: 10.1063/1.4961025

[3] J.A. Del Alamo, D.A. Antoniadis, J. Lin, W. Lu, A. Vardi, X. Zhao. IEEE J. Electron. Dev. Soc., **4**, 205 (2016). DOI: 10.1109/JEDS.2016.2571666
[4] J.A. del Alamo. Nature, **479**, 317 (2011). DOI: 10.1038/nature10677
[5] H. Riel, L.-E. Wernersson, M. Hong, J.A. del Alamo. MRS Bull., **39**, 668 (2014). DOI: 10.1557/mrs.2014.137
[6] Z. Wang, A. Abbasi, U. Dave, A. De Groote, S. Kumari, B. Kunert, C. Merckling, M. Pantouvaki, Y. Shi, B. Tian, K. Van Gasse, J. Verbist, R. Wang, W. Xie, J. Zhang, Y. Zhu, J. Bauwelinck, X. Yin, Z. Hens, J. Van Campenhout, B. Kuyken, R. Baets, G. Morthier, D. Van Thourhout, G. Roelkens. Laser Photon. Rev., **11**, 1700063 (2017). DOI: 10.1002/lpor.201700063
[7] H.-C. Wang, T.-Y. Tang, C.C. Yang, T. Malinauskas, K. Jarasiunas. Thin Solid Films, **519**, 863 (2010). DOI: 10.1016/j.tsf.2010.08.149
[8] J. Lu, X. Zheng, M. Guidry, D. Denninghoff, E. Ahmadi, S. Lal, S. Keller, S.P. DenBaars, U.K. Mishra. Appl. Phys. Lett., **104**, 092107 (2014). DOI: 10.1063/1.4867508
[9] S. Keller, N.A. Fichtenbaum, M. Furukawa, J.S. Speck, S.P. DenBaars, U.K. Mishra. Appl. Phys. Lett., **90**, 191908 (2007). DOI: 10.1063/1.2738381
[10] A.M. Mizerov, S.A. Kukushkin, Sh.Sh. Sharofidinov, A.V. Osipov, S.N. Timoshnev, K.Yu. Shubina, T.N. Berezovskaya, D.V. Mokhov, A.D. Buravlev. Phys. Solid State, **61**, 2277 (2019). DOI: 10.1134/S106378341912031X
[11] Y. Wu, X. Liu, A. Pandey, P. Zhou, W.J. Dong, P. Wang, J. Min, P. Deotare, M. Kira, E. Kioupakis, Z. Mi. Prog. Quantum Electron., **85**, 100401 (2022). DOI: 10.1016/j.pquantelec.2022.100401
[12] A.M. Mizerov, P.N. Kladko, E.V. Nikitina, A.Yu. Egorov. Semiconductors, **49**, 274 (2015). DOI: 10.1134/S1063782615020177
[13] L. Goswami, R. Pandey, G. Gupta. Appl. Surf. Sci., **449**, 186 (2018). DOI: 10.1016/j.apsusc.2018.01.287
[14] P.V. Seredin, H. Leiste, A.S. Lenshin, A.M. Mizerov. Appl. Surf. Sci., **508**, 145267 (2020). DOI: 10.1016/j.apsusc.2020.145267
[15] P.V. Seredin, D. Goloshchapov, A.O. Radam, A.S. Lenshin, N.S. Builov, A.M. Mizerov, I.A. Kasatkin. Opt. Mater., **128**, 112346 (2022). DOI: 10.1016/j.optmat.2022.112346
[16] A.M. Mizerov, S.N. Timoshnev, M.S. Sobolev, E.V. Nikitina, K.Yu. Shubina, T.N. Berezovskaia, I.V. Shtrom, A.D. Bouravleuv. Semiconductors, **52**, 1529 (2018). DOI: 10.1134/S1063782618120175
[17] A.M. Mizerov, S.N. Timoshnev, E.V. Nikitina, M.S. Sobolev, K.Yu. Shubin, T.N. Berezovskaia, D.V. Mokhov, W.V. Lundin, A.E. Nikolaev, A.D. Bouravleuv. Semiconductors, **53**, 1187 (2019). DOI: 10.1134/S1063782619090112
[18] S.A. Kukushkin, A.V. Osipov, N.A. Feoktistov. Phys. Solid State, **56**, 1507 (2014). DOI: 10.1134/S1063783414080137
[19] N. Yamabe, H. Shimomura, T. Shimamura, T. Ohachi. J. Cryst. Growth, **311**, 3049 (2009). DOI: 10.1016/j.jcrysgro.2009.01.076
[20] A.M. Mizerov, V.N. Jmerik, P.S. Kop'ev, S.V. Ivanov. Phys. Status Solidi C, **7**, 2046 (2010). DOI: 10.1002/pssc.200983488
[21] K.Y. Shubina, D.V. Mokhov, T.N. Berezovskaya, E.V. Nikitina, A.M. Mizerov. J. Phys. Conf. Ser., **1851**, 012004 (2021). DOI: 10.1088/1742-6596/1851/1/012004
[22] K.Y. Shubina, D.V. Mokhov, T.N. Berezovskaya, E.V. Pirogov, A.V. Nashchekin, S.S. Sharofidinov, A.M. Mizerov. J. Phys. Conf. Ser., **2086**, 012037 (2021). DOI: 10.1088/1742-6596/2086/1/012037
[23] https://www.ioffe.ru/SVA/
[24] S. Kukushkin, A. Osipov, V. Bessolov, B. Medvedev, V. Nevolin, K. Tcarik. Rev. Adv. Mater. Sci., **17**, 1 (2008)
[25] S.A. Kukushkin, A.V. Osipov. J. Phys. D: Appl. Phys., **47**, 313001 (2014). DOI: 10.1088/0022-3727/47/31/313001
[26] S.A. Kukushkin, A.V. Osipov. Condensed matter and interphase boundaries, **24**, 406 (2022). DOI: 10.17308/kcmf.2022.24/10549
[27] V.V. Kidalov, S.A. Kukushkin, A. Osipov, A. Redkov, A.S. Grashchenko, I.P. Soshnikov. Mater. Phys. Mech., **36**, 39 (2018). DOI: 10.18720/MPM.3612018_4
[28] S.A. Kukushkin, A.V. Osipov, V.N. Bessolov, E.V. Konenkova, V.N. Panteleyev. FTT **59**, 660 (2017) (in Russian). DOI: 10.21883/FTT.2017.04.44266.287
[29] V.S. Harutyunyan, A.P. Aivazyan, E.R. Weber, Y. Kim, Y. Park, S.G. Subramanya. J. Phys. Appl. Phys., **34**, A35 (2001). DOI: 10.1088/0022-3727/34/10A/308
[30] H.-P. Lee, J. Perozek, L.D. Rosario, C. Bayram. Sci. Rep., **6**, 37588 (2016). DOI: 10.1038/srep37588
[31] S.K. Jana, P. Mukhopadhyay, S. Ghosh, S. Kabi, A. Bag, R. Kumar, D. Biswas. J. Appl. Phys., **115**, 174507 (2014). DOI: 10.1063/1.4875382
[32] P.V. Seredin, A.V. Glotov, E.P. Domashevskaya, I.N. Arsentyev, D.A. Vinokurov, I.S. Tarasov. Appl. Surf. Sci., **267**, 181 (2013). DOI: 10.1016/j.apsusc.2012.09.053
[33] P.V. Seredin, A.V. Glotov, V.E. Ternovaya, E.P. Domashevskaya, I.N. Arsentyev, L.S. Vavilova, I.S. Tarasov. Semiconductors, **45** (11), 1433 (2011). DOI: 10.1134/S1063782611110236
[34] P.V. Seredin, A.V. Glotov, V.E. Ternovaya, E.P. Domashevskaya, I.N. Arsentyev, D.A. Vinokurov, A.L. Stankevich, I.S. Tarasov. Semiconductors, **45** (4), 481 (2011). DOI: 10.1134/S106378261104021X
[35] P.V. Seredin, H. Leiste, A.S. Lenshin, A.M. Mizerov. Results Phys., **16**, 102919 (2020). DOI: 10.1016/j.rinp.2019.102919
[36] P.V. Seredin, A.S. Lenshin, D.S. Zolotukhin, I.N. Arsentyev, D.N. Nikolaev, A.V. Zhabotinskiy. Phys. B Condens. Matter., **530**, 30 (2018). DOI: 10.1016/j.physb.2017.11.028
[37] Tauc J. Prog. Semicond. Heywood Lond., **9**, 87 (1965).
[38] P.V. Seredin, A.S. Lenshin, A.M. Mizerov, H. Leiste, M. Rinke. Appl. Surf. Sci., **476**, 1049 (2019). DOI: 10.1016/j.apsusc.2019.01.239
[39] S. Bakalova, A. Szekeres, M. Anastasescu, M. Gartner, L. Duta, G. Socol, C. Ristoscu, I.N. Mihailescu. J. Phys. Conf. Ser., **514**, 012001 (2014). DOI: 10.1088/1742-6596/514/1/012001
[40] N. Sharma, S. Sharma, K. Prabakar, S. Amirthapandian, S. Ilango, S. Dash, A.K. Tyagi. (2015). DOI: 10.48550/ARXIV.1507.04867
[41] A.M. Alsaad, Q.M. Al-Bataineh, I.A. Qattan, A.A. Ahmad, A. Ababneh, Z. Albataineh, I.A. Aljarrah, A. Telfah. Front. Phys., **8**, 115 (2020). DOI: 10.3389/fphy.2020.00115
[42] K.M. Lee, J.Y. Hwang, B. Urban, A. Singh, A. Neogi, S.K. Lee, T.Y. Choi. Solid State Commun., **204**, 16 (2015). DOI: 10.1016/j.ssc.2014.11.020
[43] W. Shan, J.W. Ager, K.M. Yu, W. Walukiewicz, E.E. Haller, M.C. Martin, W.R. McKinney, W. Yang. J. Appl. Phys., **85**, 8505 (1999). DOI: 10.1063/1.370696

[44] E. Serban, J. Palisaitis, M. Junaid, L. Tengdelius, H. Högberg, L. Hultman, P. Persson, J. Birch, Ch.-L. Hsiao. Energies, **10**, 1322 (2017). DOI: 10.3390/en10091322
[45] G.L. Zhao, D. Bagayoko. New J. Phys., **2**, 16 (2000). DOI: 10.1088/1367-2630/2/1/316
[46] A. Arvanitopoulos, N. Lophitis, S. Perkins, K.N. Gyftakis, M. Belanche Guadas, M. Antoniou. In: *2017 IEEE 11th Int. Symp. Diagn. Electr. Mach. Power Electron. Drives SDEMPED* (IEEE, Tinos, Greece, 2017), p. 565–571. DOI: 10.1109/DEMPED.2017.8062411
[47] N. Aggarwal, S. Krishna, L. Goswami, S.K. Jain, A. Pandey, A. Gundimeda, P. Vashishtha, J. Singh, S. Singh, G. Gupta. SN Appl. Sci., **3**, 291 (2021). DOI: 10.1007/s42452-021-04274-4
[48] H. Angerer, D. Brunner, F. Freudenberg, O. Ambacher, M. Stutzmann, R. Höpler, T. Metzger, E. Born, G. Dollinger, A. Bergmaier, S. Karsch, H.-J. Körner. Appl. Phys. Lett., **71**, 1504 (1997). DOI: 10.1063/1.119949
[49] Y. Turkulets, N. Shauloff, O.H. Chaulker, Y. Shapira, R. Jelinek, I. Shalish. Surf. Interfaces, **38**, 102834 (2023). DOI: 10.1016/j.surfin.2023.102834

Translated by A.Akhtyamov